Electronic structure and plasma excitations at the surface of small voids in jellium

King-Sun David Wu and D. E. Beck
Department of Physics and Laboratory for Surface Studies, University of Wisconsin–Milwaukee, Milwaukee, Wisconsin 53201
(Received 12 January 1987)

Calculation of the electronic structure and plasma excitations at the surfaces of microscopic voids in a metal are reported. The electronic structure is computed using a jellium model for the conduction electrons of a metal and the local-density-functional formalism. The excitation of this electronic system is treated by using a truncated ("long-wavelength") version of the random-phase approximation. The surface plasma excitations are a prominent feature of the electron-energy-loss spectra of rare-gas bubbles in aluminum and, hence, an understanding of these excitations can aid in the characteristics of the gas-filled voids that form in irradiated metals. Our calculations are for voids with radii of 4, 7, 14, and 20 a.u. and metallic densities with $r_s = 2$, 4, and 6 a.u.

I. INTRODUCTION

Several recent experimental studies[1–5] have reported electron-energy-loss spectroscopy studies of helium and other rare-gas bubbles in aluminum.[6] These bubbles are formed when the metal is irradiated with neutrons or ions, and they result in a swelling and deterioration of the metal structure. Hence, the characterization of the number, size, and structure of these bubbles provides important information concerning the integrity of metal structures in radiation environments. The interaction of electrons or photons with these bubbles results in excitations of the gas in the bubble and plasma excitations at the metal surface[7–10] surrounding the gas. Here we report calculations of electronic structure at the surface of microscopic voids in a metal and the plasma excitations at the surface of these voids.

We employ the widely used jellium model to describe the behavior of the conduction electrons in a metal. In this model the ions are replaced by a uniform positive background of charge into which the interacting electrons are introduced. The ground-state properties of the interacting electrons are obtained using the density-functional formalism[11] with a local-density approximation (LDA) for the exchange-correlation energy.[12] This model has been used very successfully in computing the electronic structure and response for other inhomogeneous electron systems,[13] i.e., metal surfaces[14,15] and metal particles.[16,17]

The self-consistent procedure[12] for the solution of the LDA requires extensive computations. However, this formalism readily admits computationally simpler variational procedures, and we use the procedure introduced by Rose and Shore[18] which permits a quantum-mechanical calculation of the kinetic energy of the electrons. Their procedure employs a model potential and for metal spheres has been found to give results[19] in very good agreement with those obtained using the self-consistent procedures.[16] We employ single-step model (SSM), double-step model (DSM) and rigid-sphere model (RSM) potentials in order to model the exclusion of the conduction electrons of the metal from the region of the void. The infinite-barrier potential has been widely used as a model for a metal surface, and we have included the corresponding RSM in our considerations for comparison purposes. In addition, one might argue that it should be a good model for the helium-filled void where the helium atoms prevent the metallic electrons from diffusing into the void. The LDA calculations of the electron density profiles at the surface of voids in jellium are reported in Sec. II.

The frequencies of the plasma excitations at a void surface depend on the size of the void.[3] The classical model for a void in a metal where the positive and negative charge densities coincide results in multipolar plasma excitations at frequencies[7,10]

$$\omega_L^C = \omega_p \left[\frac{L+1}{2L+1} \right]^{1/2} , \tag{1}$$

which are independent of the void radius. These modes are obtained by solving Laplace's equation for a spherical void in a metal with a frequency-dependent dielectric constant

$$\epsilon(\omega) = 1 - (\omega_p/\omega)^2 . \tag{2}$$

Here the bulk plasma frequency is $\omega_p^2 = 4\pi n_0 e^2/\mathrm{m}$ (we use atomic units where $e = \hbar = m = 1$; the length unit is the Bohr radius and the energy unit is 27.2 eV). The introduction of spatial dispersion into the electromagnetic response[10,20] or a surface electronic profile into the local dielectric constant[10] results in a radial dependence for the computed frequencies. A spatially dependent local dielectric constant is obtained by replacing n_0 in ω_p^2 in Eq. (2) by an inhomogeneous electron density $n(r)$:

$$\epsilon(\omega, r) = 1 - (\omega_p/\omega)^2 [n(r)/n_0] . \tag{3}$$

Computations using this local approximation predict an increase in plasma frequencies for decreasing void radius[10,21]—"blue shift," $\omega_L > \omega_L^C$.

Aers *et al.*[10] have reported calculations for voids using model surface density profiles. Their hydrodynamic calculations include spatial dispersion, and investigate the effects of surface inhomogeneity by using a stepped electron density profile with an intermediate density step

 ©1987 The American Physical Society

(height and width are varied) to model the electronic profile at the void surface. The random-phase approximation provides a quantum-mechanical computation of the linear response of an electronic system, and Lushnikov *et al.*[20] have employed a truncated version of this approximation (TRPA) in the computation of the response of small metal spheres. The TRPA gives the same formal results for the plasma frequencies[10] and shares the computational advantage enjoyed by the hydrodynamic approach, since it requires only the ground-state electronic density and not the quantum-mechanical response of the electrons. In Sec. III, we report a TRPA calculation of the plasma frequencies for voids using the electronic density profiles reported in Sec. II. The computed frequencies for $L=1$ are compared to the experimental results in the concluding section of this paper, Sec. IV.

II. ELECTRON DENSITY PROFILE AT A VOID SURFACE

Our computation of the electron density profile at the surface of a spherical void in a metal is performed using the LDA.[11,12] In this formalism the ground-state energy of a system of electrons in the presence of an external potential $v(\mathbf{r})$ is a functional of the electron density:

$$E[n]=\int d\mathbf{r}\, v(\mathbf{r})n(\mathbf{r})+\tfrac{1}{2}\int d\mathbf{r}\int d\mathbf{r}'\frac{n(\mathbf{r})n(\mathbf{r}')}{|\mathbf{r}-\mathbf{r}'|}+\int d\mathbf{r}\,\varepsilon_{\rm xc}(\mathbf{r})n(\mathbf{r})+T_s[n]\ , \tag{4}$$

which is a minimum for the exact electron density. The local-density expressions[14]

$$\varepsilon_x[n]=-3/4(3n/\pi)^{1/3}$$

and

$$\varepsilon_c[n]=-0.44/[(3/4\pi n)^{1/3}+7.8]$$

are used for the exchange-correlation energy $\varepsilon_{xc}(\mathbf{r})$ which permits us to compare our profiles to those obtained for a flat metal surface by Lang and Kohn.[14]

The jellium model of the conduction electrons in a metal is used, hence the external potential is provided by a uniform positive charge density which replaces the ion cores of the metal atoms. For a spherical void of radius R, this charge density if given by $n^+(\mathbf{r})=n_0\Theta(r-R)$ where $\Theta(r)$ is the unit step function, $n_0=3/4\pi r_s^3$, and r_s characterizes the bulk conduction electron density. Introducing the electrostatic energy of this positive charge density interacting with itself, we can rewrite the electrostatic contributions to the ground-state energy in a compact and finite expression:[22]

$$E_{\rm es}[n]=\tfrac{1}{2}\int d\mathbf{r}\int d\mathbf{r}',\frac{\Delta n(\mathbf{r})\Delta n(\mathbf{r}')}{|\mathbf{r}-\mathbf{r}'|}\ , \tag{5}$$

where

$$\Delta n(\mathbf{r})=n(\mathbf{r})-n^+(\mathbf{r})\ .$$

The final term in the energy functional, $T_s[n]$, accounts for the kinetic energy of the electrons. The Kohn-Sham self-consistent procedure employs a Schrödinger equation for the noninteracting particles subject to an effective density-dependent potential. The electron density is given in terms of the particle wave functions,

$$n(\mathbf{r})=\sum_{\text{occupied}}|\psi_i(\mathbf{r})|^2\ , \tag{6}$$

and the kinetic energy is computed using

$$T_s[n]=-\sum_{\text{occupied}}\left\langle\psi_i\left|\frac{\nabla^2}{2}\right|\psi_i\right\rangle\ . \tag{7}$$

Obtaining the self-consistent density requires extensive numerical computations, and the energy functional readily admits computationally simpler variational calculations. Rose and Shore[18] introduced a variational density by employing a model potential, $V(\mathbf{r},\alpha)$. Solution of Schrödinger's equation for noninteracting particles in this variational potential then permits the retention of the quantum-mechanical expression, (7), for the kinetic energy. The energy functional is minimized by varying the potential parameters here denoted by α. A number of the details associated with the numerical evaluation of the energy functional for large r and angular momentum have been collected in Appendix A.

We have carried through the variational calculation for two spherically symmetric model potentials for which Schrödinger's equation can be solved analytically:[23]

(i) A single-step model (SSM),

$$V_1(\mathbf{r},\alpha)=V_0\Theta(r_0-r)\ ,$$

where the parameters are the step height V_0 and the location of the step edge r_0.

(ii) A double-step model (DSM),

$$V_2(\mathbf{r},\alpha)=V_0\Theta(r_0-r)+V_s[\Theta(r_1-r)-\Theta(r_0-r)]\ ,$$

with the additional parameters V_s and r_1.

The total charge of the system must be zero so there is a constraint on the allowed variational densities, and this constraint is used to fix the position of the model potential, r_0, with respect to the positive background. For the SSM the single free variational parameter is the step height V_0. For the DSM we have three free variational parameters, V_0, V_s, and the width, $w=r_1-r_0$, of the intermediate step. Fortunately, the energy is not strongly dependent on this width so that it is possible to minimize the functional without recourse to an elaborate search scheme. We have also computed the electron density for the rigid-sphere model which corresponds to the much-used "infinite-barrier" model for a metal surface.

(iii) Rigid-sphere model (RSM),

$$V(\mathbf{r})=\begin{cases}\infty & \text{for } r<r_0\ ,\\ 0 & \text{for } r>r_0\ ,\end{cases}$$

where r_0 is fixed by the constraint of charge neutrality.

The model potential parameters obtained for voids of radii $R=4$, 7, 14, and 20 a.u. and positive background densities corresponding to $r_s=2$, 4, and 6 a.u. are presented in Table I for the SSM and RSM and in Table II for the DSM. The three free variational parameters for the DSM potential complicate the search for the energy

TABLE I. Model potential parameters for the SSM and RSM potentials for voids in jellium. All quantities are in atomic units.

			$R=4$	$R=7$	$R=14$	$R=20$
$r_s=2$	SSM	V_0	0.285	0.383	0.427	0.441
		r_0	4.370	7.166	14.0736	20.045
	RSM	r_0	2.876	5.834	12.804	18.792
$r_s=4$	SSM	V_0	0.086	0.112	0.132	0.130
		r_0	4.168	6.962	13.76	19.778
	RSM	r_0	1.956	4.782	11.664	17.663
$r_s=6$	SSM	V_0	0.039	0.061	0.077	0.090
		r_0	4.106	6.621	13.23	18.943
	RSM	r_0	2.168	3.859	10.584	16.502

minimum. However, the total energy is not very sensitive to the height of the internal step, V_0, or the width w of the intermediate step, so that one can employ a coarse mesh for these two variational parameters. The total energy for the metallic densities with $r_s=4$ and 6 are only slightly lowered by the increased variational freedom introduced in going from the SSM to the DSM. For the higher-density system with $r_s=2$, the electrostatic contribution to the total energy is more nearly equal in magnitude to the kinetic and exchange-correlation contributions, and the energy is more sensitive to the model potential.

Note that for $r_s=6$, we obtain a negative value for the height of the intermediate step, V_s. For this density there are prominent Friedel oscillations at the void surface which result in a valley in the effective potential.[14] These larger oscillations reflect the larger electronic charge buildup at the surface which is needed in order to screen the void with a sparser bulk density.

In Fig. 1 the computed electron densities at the surface of a void of radius $R=20$ a.u. are presented for metals with conduction electron densities corresponding to $r_s=2$, 4, and 6 a.u. The densities for the DSM and RSM calculations are present along with the self-consistent Lang-Kohn densities[14] for a flat metal surface—the SSM densities are not presented, since they are almost identical to the DSM densities. These figures show that there is good agreement between the self-consistent Lang-Kohn profiles and those obtained using the DSM. The Friedel oscillations fall off more rapidly with increasing r for the void profiles than they do for the flat surface profiles. However, this should be attributed to the difference in geometry and not to the difference in calculational procedures. The density profiles for the RSM computation show the effect of the infinite barrier in that the density drops rapidly within the void.

The variation in density profile due to void size can be seen in the electronic profiles shown in Fig. 2. Each figure contains the computed profile for spheres of radii 4, 7, and 14 a.u. For the smallest voids the electron density is large within the void and there is a corresponding decrease in the amplitude of the Friedel oscillations in the model. These profiles were computed using the DSM potential, and the almost identical profiles were obtained in the SSM calculations—the lower step height in the SSM results in a slightly larger electron density in the void.

III. PLASMA EXCITATIONS AT THE VOID SURFACE

Ehrenreich and Cohen's development of the random-phase approximation[24] as a self-consistent field has facilitated the application of this approximation for the linear response of a system to inhomogeneous systems.[15] The

TABLE II. Model potential parameters for the DSM potential for voids in jellium. All quantities are in atomic units.

		$R=4$	$R=7$	$R=14$	$R=20$
$r_s=2$	V_0	0.40	0.52	0.52	0.52
	r_0	3.085	5.998	12.496	18.468
	V_s	0.167	0.139	0.231	0.241
	w	1.6	1.9	2.1	2.1
$r_s=4$	V_0	0.15	0.16	0.17	0.18
	r_0	1.895	4.881	11.690	17.598
	V_s	0.066	0.071	0.085	0.091
	w	2.5	2.5	2.5	2.5
$r_s=6$	V_0	0.029	0.061	0.063	0.070
	r_0	4.883	6.884	14.091	19.800
	V_s	−0.00076	−0.001	−0.0026	−0.0021
	w	5.0	5.0	5.0	7.0

density disturbance associated with the excitation of the electronic system is given by

$$\delta n(\mathbf{r},\omega)=\int d\mathbf{r}'\chi(\mathbf{r},\mathbf{r}';\omega)\delta v(\mathbf{r}',\omega) , \tag{8}$$

where the generalized susceptibility is

$$\chi(\mathbf{r},\mathbf{r}';\omega)=\sum_{\mathbf{k},\mathbf{k}'}\psi_{\mathbf{k}}(\mathbf{r})\psi_{\mathbf{k}}^{*}(\mathbf{r})\frac{f_{\mathbf{k}}-f_{\mathbf{k}'}}{\varepsilon_{\mathbf{k}}-\varepsilon_{\mathbf{k}'}+\omega}\psi_{\mathbf{k}'}(\mathbf{r}')\psi_{\mathbf{k}}^{*}(\mathbf{r}') .$$

Here $\psi_{\mathbf{k}}(\mathbf{r})$ is the wave function for an electron with an energy $\varepsilon_{\mathbf{k}}$ and $f_{\mathbf{k}}$ is the Fermi distribution function. The electrostatic potential induced by the density perturbation is obtained from Poisson's equation,

$$\delta v(\mathbf{r})=\int d\mathbf{r}\frac{\delta n(\mathbf{r}')}{|\mathbf{r}-\mathbf{r}'|} . \tag{9}$$

Taking the electron wave function to be real and rearranging the expression for $\chi(\mathbf{r},\mathbf{r}',\omega)$ one easily obtains

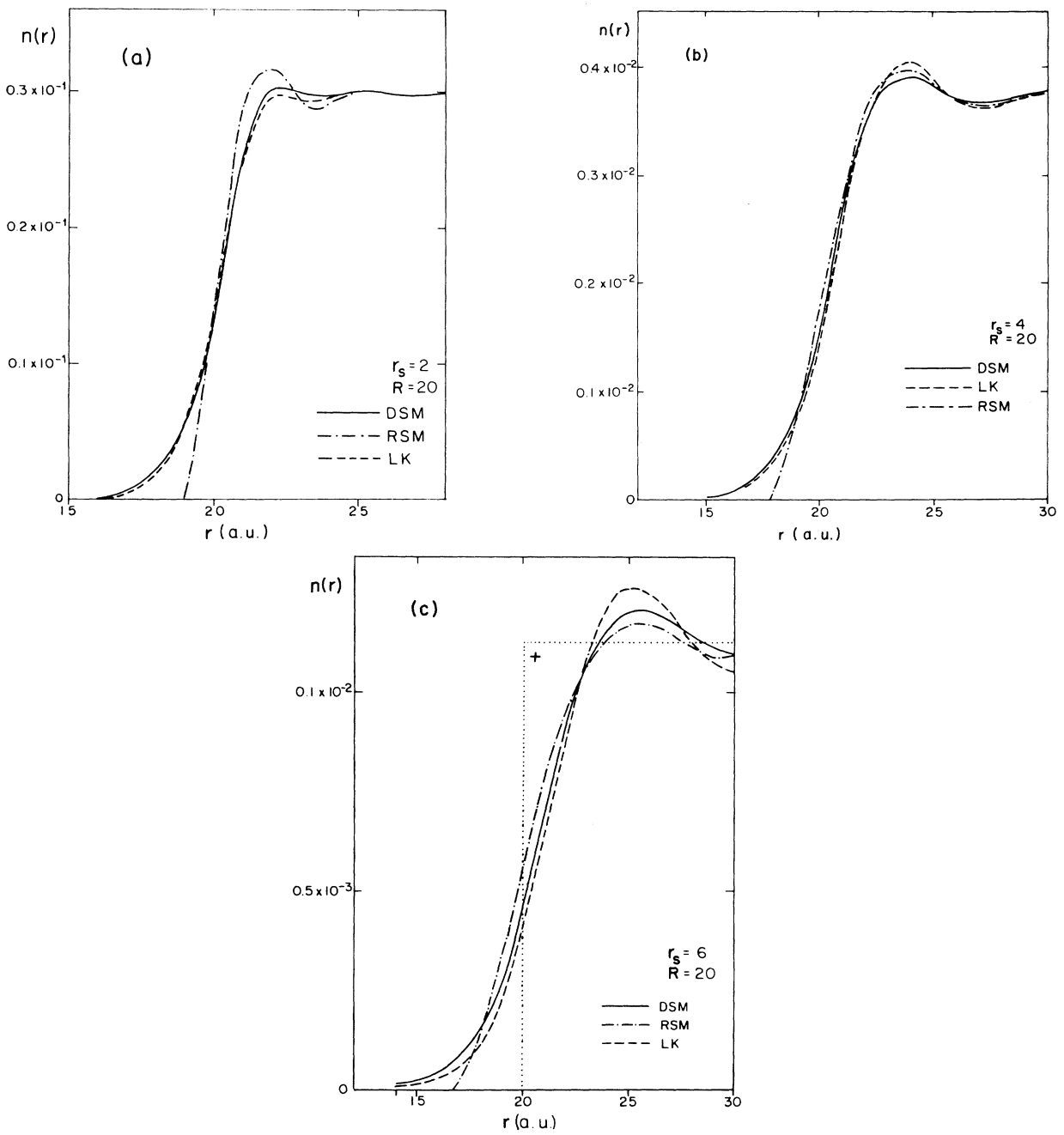

FIG 1. Electron density profiles at the surface of voids of radius $R=20$ a.u. The profiles were obtained in the DSM and RSM calculations, and they are compared with the Lang-Kohn profiles, Ref. 14, for flat jellium surfaces.

$$\chi(\mathbf{r},\mathbf{r}';\omega)=2\sum_{\mathbf{k},\mathbf{k}'} f_{\mathbf{k}}\psi_{\mathbf{k}}(\mathbf{r})\psi^*_{\mathbf{k}'}(\mathbf{r})\frac{\epsilon_{\mathbf{k}}-\epsilon_{\mathbf{k}'}}{(\epsilon_{\mathbf{k}}-\epsilon_{\mathbf{k}'})^2-\omega^2}\psi_{\mathbf{k}'}(\mathbf{r}')\psi^*_{\mathbf{k}}(\mathbf{r}') \ . \tag{10}$$

Setting $\epsilon_{\mathbf{k}}=k^2/2m$ and $\mathbf{k}'=\mathbf{k}+\mathbf{q}$, we have $\epsilon_{\mathbf{k}}-\epsilon_{\mathbf{k}'}=\mathbf{q}\cdot\mathbf{k}/m$. For a flat surface one can take $\mathbf{q}$ to be a vector along the surface and associate it with the wave vector for the surface plasma excitation—for this problem one finds (after a great deal of manipulation) that the susceptibility can be expanded in powers of q—long-wavelength approximation.

Lushinikov *et al.*[20] in their treatment of the metal-sphere problem argue that, since $|\mathbf{k}|<k_F$ (k_F is the Fermi wave number), and the wavelength for a distrubance on the sphere surface should be of order R, the susceptibility can be expanded in powers of q^2/ω^2. Their estimate of the validity of this expansion is given by considering

$$\frac{qk_F}{m\omega_P}\approx\frac{2\pi}{\lambda}\sqrt{3}r_{\mathrm{TF}}=\sqrt{3}\frac{r_{\mathrm{TF}}}{R} \ ,$$

where the Thomas-Fermi screening length is given by $r^2_{\mathrm{TF}}=\pi/4me^2k_F$ and λ has been set equal to $2\pi R$. For $r_s=2$ and $R=4$ this ratio has a value of 0.4. They proceed by requiring that $(|\epsilon_{\mathbf{k}}-\epsilon_{\mathbf{k}'}|/\omega)^2<1$ and retaining only the leading term in a power-series expansion of Eq. (10) in this ratio. The great advantage of this TRPA is that the linear-response relation between the induced density and potential, Eq. (8), can be reduced to[20]

$$\delta n(\mathbf{r},\omega)=-(e^2/m\omega^2)\nabla\cdot[n(\mathbf{r})\nabla\delta v(\mathbf{r},\omega)] \ , \tag{11}$$

which depends only on the ground-state electron density.

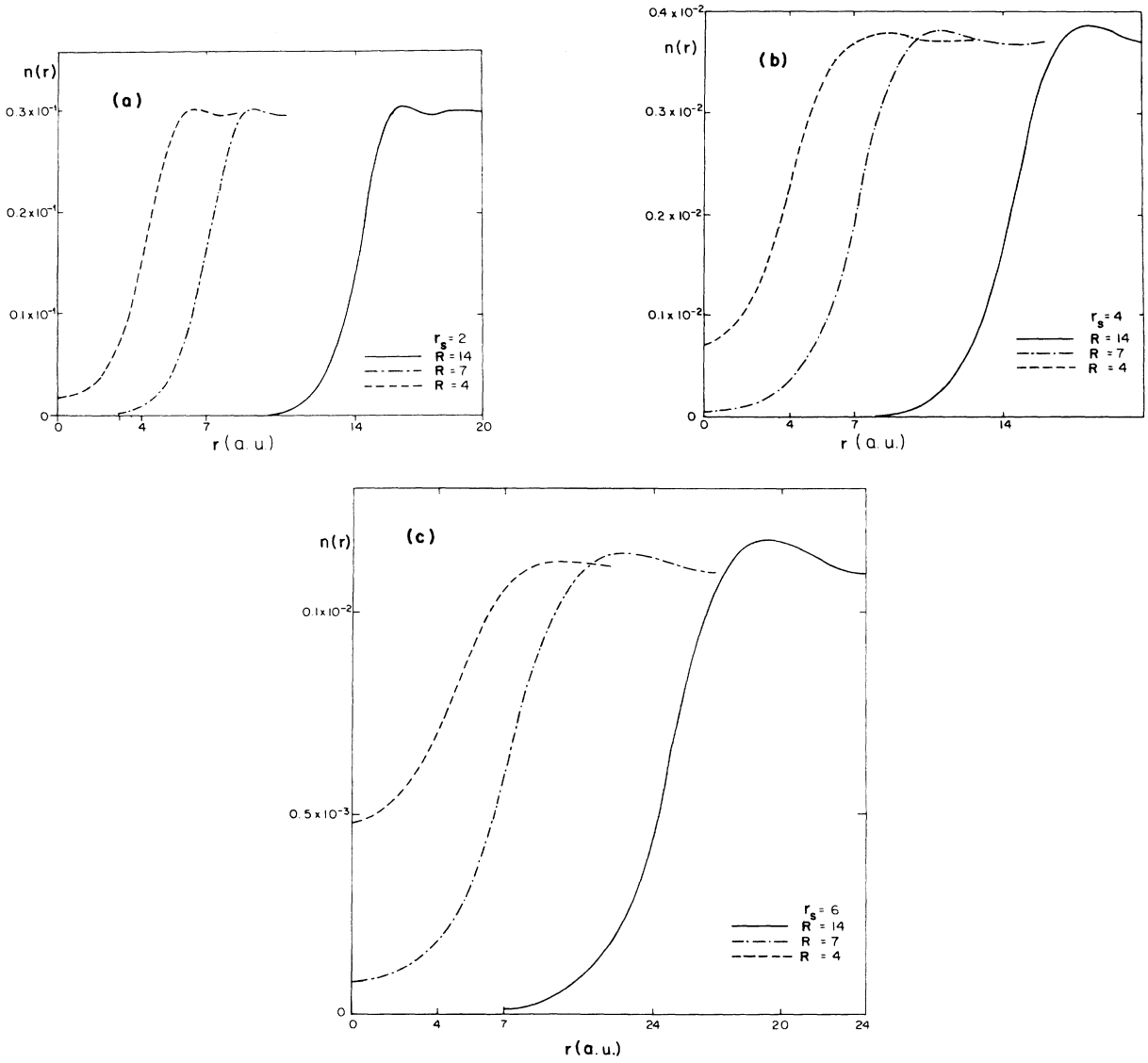

FIG 2. Comparison of the electron density profiles for voids of radii 4, 7, and 14 a.u. in jellium. The profiles were calculated using the DSM.

Expanding the induced potential and density in partial waves,

$$\delta v(\mathbf{r},\omega)=\sum_L Y_L^0(\hat{\mathbf{r}})v_L(r,\omega) ,$$

where $Y_L^0(\hat{\mathbf{r}})$ is a spherical harmonic, and substituting Eq. (9) into Eq. (11) one obtains the integral equation

$$\omega^2 v_L(r,\omega)=\eta(r)v_L(r,\omega)-\int r'^2 dr K_L(r,r')v_L(r',\omega) , \quad (12)$$

for a spherically symmetric density $n(r)$. Here we have set $\eta(r)=4\pi e^2 n(r)/m$, and

$$K_L(r,r')=\frac{1}{2L+1}\frac{\partial}{\partial r'}\left[\frac{r^{<L}}{r^{>L+1}}\right]\frac{\partial}{\partial r'}n(r') .$$

If we consider a step electron density profile, $n(r)=n_0\Theta(r-R)$, then $\partial n/\partial r=n_0\delta(r-R)$, and we can easily integrate Eq. (12) to obtain

$$v_L(r,\omega)=\begin{cases}\left[\left[\frac{\omega_p}{\omega}\right]^2\left[\frac{L+1}{2L+1}\right]\left[\frac{r}{R}\right]^L v_L(R,\omega) & \text{for } r<R ,\\ \left[1-\left[\frac{\omega}{\omega_p}\right]^2\right]^{-1}\frac{L}{2L+1}\left[\frac{R}{r}\right]^{L+1} v_L(R,\omega) & \text{for } r>R,\end{cases}$$

which supports the classic surface plasma modes ω_L^c, in Eq. (1). Also note that the induced density, $n_L(r,\omega)\propto\delta(r-R^+)$, is completely localized at the void surface.

The insight derived from the simple solution above aided us in establishing a stable iteration scheme for the self-consistent solution of the integral equation for $v_L(r,\omega)$. The radial dependence is divided into two regions with a matching point r_m determined by the condition

$$\eta(r_m)=\omega^2$$

for the frequency being considered. For $r<r_m$ the jth iteration for $v_L(r,\omega)$ is substituted into the right-hand side of Eq. (12) in order to obtain the $(j+1)$th iteration. For $r>r_m$ we rearrange Eq. (12) and use

$$v_L^{(j+1)}(r,\omega)\eta(r)=\omega^2 v_L^{(j)}(r,\omega)+\int r'^2 dr' K_L(r,r')v_L^{(j)}(r',\omega) .$$

These expressions are iterated to self-consistency for a particular ω, however, only for a plasma mode frequency (eigenfrequency) is the resulting induced potential continuous at the matching point. Additional constraints on the solutions to the integral equation, which may be used to obtain the eigenfrequencies, are that at $r=r_m$ the integral term in Eq. (12) must be zero and that

$$\frac{\partial}{\partial r}v_L(r,\omega)\bigg|_{r_m}=0 ,$$

which is easily shown from Eq. (11) and Poisson's equation.

We employ the electron density profiles obtained from the DSM and RSM calculations described in Sec. II to compute the plasma mode frequencies which are given in Table III for $L=1$ and 2. These frequencies increase toward the bulk plasma frequency as the void radius decreases. This "blue shift" is a result of the diffuse electronic density at the void surface and the buildup of the electron density within the void for very small voids. This same reasoning also accounts for the enhancement in this blue shift in the lowest-density metallic system ($r_s=6$). The surface profiles are sharper for a RSM calculation and result in a smaller shift with decreasing void size.

In Fig. 3 we show the perturbed electron density associated with an $L=1$ plasma mode. This density disturbance is highly peaked at r_m and well localized at the surface. We expect the localization at the surface to be pronounced, however, the extreme sharpness of the response seen here probably results from the use of TRPA.

IV. CONCLUDING REMARKS

Our density-functional calculation of the electron density profiles at the surface of spherical voids in jellium confirms the quantum-mechanical expectations for these surface densities. The electrons diffuse into the void, and

TABLE III. Ratio of the square of the plasma frequency for an excitation at a void surface to the bulk plasma frequency, $(\omega_L/\omega_P)^2$, for voids in jellium. These were calculated using the TRPA and the electron density profiles from the RSM and DSM calculations. All quantities are in atomic units.

		$R=4$		$R=7$		$R=14$		$R=20$	
		$L=1$	$L=2$	$L=1$	$L=2$	$L=1$	$L=2$	$L=1$	$L=2$
$r_s=2$	RSM	0.77	0.735	0.74	0.685	0.71	0.65	0.70	0.64
	DSM	0.82	0.80	0.78	0.77	0.72	0.68	0.70	0.66
$r_s=4$	RSM	0.85	0.84	0.78	0.75	0.73	0.68	0.715	0.66
	DSM	0.875	0.855	0.80	0.77	0.74	0.69	0.72	0.67
$r_s=6$	RSM	0.875	0.87	0.83	0.81	0.75	0.71	0.73	0.68
	DSM	0.925	0.91	0.84	0.82	0.77	0.73	0.745	0.70

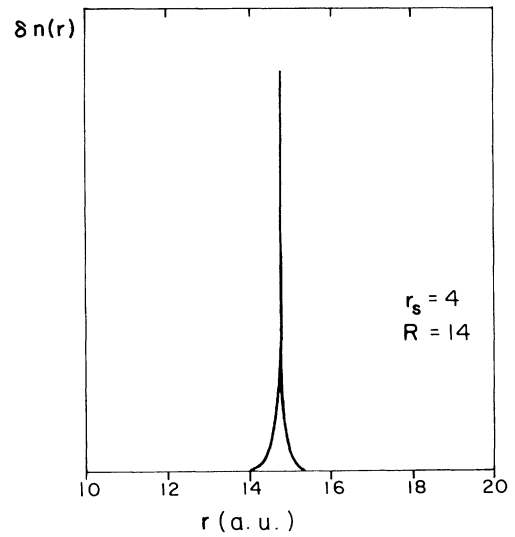

FIG. 3. The induced electron density associated with the surface plasma oscillation with $L=1$ at the surface of a void of radius 14 a.u. in jellium with $r_s=4$ a.u.

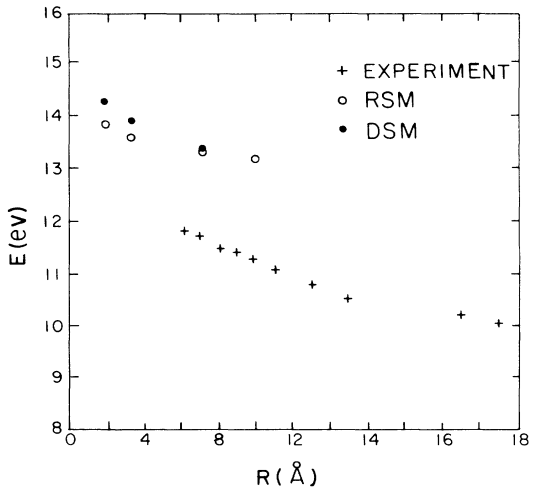

FIG. 4. Calculated surface plasma energy vs void radius for modes with $L=1$ in jellium with $r_s=2$ a.u. Electron density profiles from the RSM and DSM were used in the TRPA for these calculations. Also shown is the experimental data for the helium-filled voids in aluminum ($r_s=2.07$ a.u.) from Ref. 3. The mean void radius for the experimental data is obtained using $R_m=5.3+0.35C_{\mathrm{He}}$ Å.

the density within the void increases as the void radius decreases. This microscopic model for the electronic density at the surface of a void in a metal also facilitates the investigation of the electronic excitations at this surface.

The TRPA provides a computationally simple means of treating the response of an inhomogeneous system of electrons, however, the validity of the approximations needed to derive it are perhaps suspect for finite structures such as spheres and voids. The "blue shift" with decreasing void radius found in the TRPA is slightly larger than that found using the local dielectric constant approximation with a fixed, diffuse electron density profile.[10,21,25] This is principally due to the buildup of electrons in the void as the radius decreases. This effect is clearly illustrated by considering a solution of the classical model for a metallic sphere embedded in a metal with a higher conduction-electron density. Using the frequency-dependent dielectric constants for these metals, Eq. (2), one finds

$$(L+1)\epsilon(\omega_L)=\epsilon_S(\omega_L)L \ ,$$

or

$$\omega_L^2=[(L+1)\omega_P^2+L\omega_{PS}^2]/2L+1 \ .$$

Letting the electronic density of the embedded sphere go to zero, $\omega_{PS}\rightarrow 0$, one obtains the classical surface plasma frequency for a void, and as $\omega_{PS}\rightarrow\omega_P$, the surface plasma frequency approaches the bulk plasma frequency.

Recent experimental studies of helium and other rare-gas bubbles in aluminum by electron-energy-loss spectroscopy[1-5] have provided data concerning the excitation frequency for surface plasma modes in these bubbles. In Fig. 4 we have provided a comparison between our computed frequencies ($r_s=2.0$) and those reported by Manzke *et al.*[3] for helium-filled voids in aluminum ($r_s=2.07$). Their experimental parameter is the helium concentration C_{He}, and they indicate that the size distribution of the voids depends on this concentration; for instance, they quote $R_m=10\pm 5$ Å as the mean void radius at a concentration of 13%. We have fitted the interpolation formula, $R=5.3+0.35C_{\mathrm{He}}$ Å, to their data for mean radius versus concentration in order to permit a comparison of our calculations with their data.

The experimental data also shows the blue shift with decreasing void size but the experimental values have systematically lower energies. However, this comparison should be regarded as very ambitious, since there are many important differences between the experimental system and the theoretical model. The void density in the experimental samples is high enough that the van der Waals interaction[8] between voids is expected to modify the surface plasma frequency. The helium in the voids should also lower ω_L since the classical result for a void filled with a dielectric is given by

$$\omega_L^2=\frac{\omega_P^2(L+1)}{L(\epsilon_{\mathrm{He}}+1)+1} \ .$$

Since the helium pressure in the voids decrease as their radii increase, the dielectric constant decreases with radius (Manzke *et al.*[3] quote $\epsilon_{\mathrm{He}}=2.05$ for $R_m=10$ Å and $\epsilon_{\mathrm{He}}=1.56$ for $R_m=25$ Å). This produces a shift in opposition to the blue shift and should tend to "flatten" the experimental data.

APPENDIX

In this appendix we have collected a number of the details concerning the numerical computations for the density functional calculation described in Sec. II.

The radial component of the Schrödinger equation for a constant potential has the real solution[26]

$$\phi_l(k,r)= A_l[(\cos\delta_l)j_l(\kappa r)-(\sin\delta_l)n_l(\kappa r)] , \quad \text{(A1)}$$

where $j_l(\kappa r)$ and $n_l(\kappa r)$ are spherical Bessel functions of the first and second kind, $k^2=2mE$ and $\kappa^2=2m(E-V)$. For our model potentials, we have $V=0$ for large r and the asymptotic behavior of the wave function is given by

$$\phi_l(k,r)\approx A_l j_l(kr+\delta_l) . \quad \text{(A2)}$$

The spherically symmetric electron density for a given energy is

$$n(k,r)=(2s+1)\sum_{l=0}^{\infty}(2l+1)\,|\,\phi_l(k,r)\,|^2 ,$$

and the density is

$$n(r)=\sum_{k=0}^{k_F} n(k,r) .$$

Hence, we can use the identity

$$\sum_{l=0}^{\infty}(2l+1)\,|\,j_l(z)\,|^2=1$$

to subtract $n^+(r)$ from $n(r)$ and obtain

$$\Delta n(r)=\sum_{k=0}^{k_F}(2s+1)\sum_{l=0}^{l\,\max}(2l+1)[\,|\,\phi_l(k,r)\,|^2 - |\,A_l j_l(kr)\,|^2\Theta(r-R)] , \quad \text{(A3)}$$

where $l_{\max}$ is finite.

For the single-step potential we have $V=V_0$ for $r<r_0$ and $\phi_l\propto j_l(\kappa r)$ so that for $l\gg\kappa r$,

$$j_l(\kappa r)\approx\frac{(\kappa r)^l}{(2l+1)!!} .$$

Hence, for large enough l we can terminate the l summation for $r<r_0\approx R$. For $r>r_0$, we have both terms in Eq. (A1), but the matching conditions at $r=r_0$ can be used to show that for $l\gg kr_0$,[26]

$$\delta_l\approx-\frac{\epsilon_l(kr_0)^{2l+2}}{[(2l-1)!!]^2} ,$$

where $|\,\epsilon_l\,|\le(2l+1)/kr_0$ (the maximum value being the rigid-sphere result). Hence, the phase shifts decrease rapidly as l increases so that $\phi_l(k,r)\propto A_l j_l(kr)$. Therefore, we can find a $l_{\max}>k_F r_0\approx k_F R$ such that the contributions to $\Delta n(r)$ for $l>l_{\max}$ can be neglected.

For large r the net charge density has Friedel oscillations

$$\Delta n(r)\approx A\cos(k_F r+\phi)/r^3 ,$$

and the radial integral one needs for the energy, Eq. (4), converges very slowly. The contributions to these integrals for $kr>kr_c=z$ are evaluated by using a rational approximation for $f(z)$ and $g(z)$ in the sine and cosine integrals[27]

$$\int_z^{\infty}dt\frac{\sin t}{t}=f(z)\cos z+g(z)\sin z ,$$

and

$$\int_z^{\infty}dt\frac{\cos t}{t}=g(z)\cos z-f(z)\sin z .$$

The integrals needed in the calculation can then be obtained by iteration, since

$$C_n(z)=\int_z^{\infty}dt\frac{\cos t}{t^n}=\frac{1}{n-1}\left[\frac{\cos z}{z^{n-1}}-S_{n-1}(z)\right]$$

and

$$S_n(z)=\int_z^{\infty}dt\frac{\sin t}{t^n}=\frac{1}{n-1}\left[\frac{\sin z}{z^{n-1}}+C_{n-1}(z)\right] .$$

The cutoff radius used in our calculations was $r_c=R+8.0$ a.u.

[1] J. C. Rife, S. E. Donnelly, A. A. Lucas, J. M. Giles, and J. J. Ritsko, Phys. Rev. Lett. **46**, 1220 (1981).

[2] R. Manzke and M. Campagna, Solid State Commun. **39**, 313 (1981).

[3] R. Manzke, G. Crecelius, and J. Fink, Phys. Rev. Lett. **51**, 1095 (1983).

[4] A. vom Felde, J. Fink, Th. Muller-Heinzerling, J. Pfluger, B. Scheerer, G. Linker, and D. Kaletta, Phys. Rev. Lett. **53**, 922 (1984).

[5] A. vom Felde and J. Fink, Phys. Rev. B **31**, 6917 (1985).

[6] P. Henoc and L. Henry, J. Phys. (Paris) Colloq. Suppl. 4, **31**, C1-55 (1970).

[7] M. Natta, Solid State Commun. **7**, 823 (1969).

[8] A. A. Lucas, Phys. Rev. B **7**, 3527 (1973); K. Ohtaka, H. Miyazaki, and A. A. Lucas, *ibid.* **21**, 467 (1980); A. Rouveaux and A. Magnus, Solid State Commun. **34**, 695 (1980).

[9] J. C. Ashley and T. L. Ferrell, Phys. Rev. B **14**, 3277 (1976).

[10] G. C. Aers, B. V. Paranjape, and A. D. Boardman, J. Phys. Chem. Solids **40**, 319 (1979).

[11] P. Hohenberg and W. Kohn, Phys. Rev. **136**, B864 (1964).

[12] W. Kohn and L. J. Sham, Phys. Rev. **140**, A1133 (1965).

[13] A meeting abstract also refers to use of this model in the computation of the void properties: H. Yamauchi, J. Met. **36**, 67 (1984).

[14] N. D. Lang and W. Kohn, Phys. Rev. B **1**, 4555 (1970); N. D. Lang, Solid State Phys. **28**, 225 (1973).

[15] B. B. Dasgupta and D. E. Beck, in *Electromagnetic Surface Modes*, edited by A. D. Boardman (Wiley, New York, 1982), p. 77.

[16] D. E. Beck, Solid State Commun. **49**, 391 (1984); W. Ekardt, Phys. Rev. B **29**, 1558 (1984); A. Hintermann and M. Manninen, *ibid.* **27**, 7262 (1983).

[17] W. D. Knight, K. Clemenger, W. A. de Heer, W. A. Saunders, M. Y. Chou, and M. L. Cohen, Phys. Rev. Lett. **52**, 2141 (1984); W. Ekardt, *ibid.* **52**, 1925 (1984); W. Ekardt, Phys. Rev. B **31**, 6360 (1985); D. E. Beck, *ibid.* **30**, 6935 (1984); W. D. Knight, W. A. de Heer, K. Clemenger, and W. A. Saunders, Solid State Commun. **53**, 445 (1985).

[18] J. H. Rose, Jr. and H. B. Shore, Solid State Commun. **17**, 217 (1975).

[19]J. L. Martins, R. Car, and J. Buttet, Surf. Sci **106**, 265 (1981).
[20]A. A. Lushnikov and A. J. Simonov, Z. Phys. **270**, 17 (1974); V. V. Maksimenko, A. J. Simonov, and A. A. Lushnikov, Phys. Status Solidi B **82**, 685 (1977); A. A. Lushnikov, V. V. Maksimenko, and A. J. Simonov, in *Electromagnetic Surface Modes,* edited by A. D. Boardman (Wiley, New York, 1982), p. 305.
[21]K.-S. D. Wu, Ph.D. thesis, University of Wisconsin-Milwaukee, 1985.
[22]One also needs to subtract a constant term for the exchange-correlation energy of the bulk metal, $\int d\mathbf{r}\,\varepsilon_{xc}(\mathbf{r})n^{+}(\mathbf{r})$, in order to obtain a finite result for the total energy.
[23]L. I. Schiff, *Quantum Mechanics,* 3rd ed. (McGraw-Hill, New York, 1968).
[24]H. Ehrenreich and M. H. Cohen, Phys. Rev. **115**, 786 (1959).
[25]A computation employing our density profiles and the local dielectric constant approximation, Eq. (3), yields the same values for ω_L as those reported here for the TRPA.
[26]L. I. Schiff, *Quantum Mechanics,* 3rd ed. (McGraw-Hill, New York, 1968), Sec. 19.
[27]W. Gautschi and W. F. Cahill, in *Handbook of Mathematical Functions,* edited by M. Abramowitz and I. A. Stegun (National Bureau of Standards, Washington, D. C., 1964), p. 227.